CORONAL SURVEY IN X-RAYS OF O VII AND Ne IX

L. W. ACTON, R. C. CATURA, A. J. MEYEROTT† and C. J. WOLFSON
Lockheed Palo Alto Research Laboratory, Palo Alto, Calif., U.S.A.

and

J. L. CULHANE
Mullard Space Science Laboratory, Physics Dept., University College, London, England

(Received 30 March, 1972; revised 10 May, 1972)

Abstract. We report some results of a rocket experiment flown on 29 April, 1971. A survey of the solar corona was carried out with a pair of collimated Bragg spectrometers to study the resonance, intersystem and forbidden line emission from the helium-like ions O VII (22 Å) and Ne IX (13 Å). In the direction of dispersion the collimator provided a field of view of 1.7′. Also, the continuum radiation near 3 Å was monitored by a collimated proportional counter within a view angle of 4.2′. The observed X-ray emission came from the general corona, seven plage regions, and one dynamic feature – the late stage of a small flare. From the intensity of the O VII and Ne IX resonance lines the electron temperature and emission measure of the individual emitting regions are derived on the basis of two models, one (a) in which the region is assumed to be isothermal and another (b) in which the emission measure decreases exponentially with increasing temperature. The latter model, which is the most adequate of the two, yields for the electron temperature of the time-varying feature 2–3 $\times 10^6$ K, for the other active regions 1.5–2.5 $\times 10^6$ K, and for the general corona 1.3–1.7 $\times 10^6$ K. The Ne IX emitting regions are about 1.5 times as hot as the O VII regions. The emission measure ranges from 0.4–2.3 $\times 10^{48}$ cm^{-3} for all active regions and is about 2 $\times 10^{49}$ cm^{-3} for one hemisphere of the general corona above 10^6 K. From an analysis of the ratio, R, of the forbidden and intersystem lines of O VII we conclude that none of the regions producing these lines at the time of the rocket flight had electron densities exceeding about 3 $\times 10^9$ cm^{-3}. Our data demonstrate a dependence of R upon temperature in agreement with the theory of Blumenthal *et al.* (1971). The wavelengths for the intersystem, the $1s^2 2s\ ^2S^e$–$1s2p2s\ ^2P^0$ satellite, and the forbidden transition show in the case of Ne IX improved agreement with predictions.The observed strength of the satellite lines for both O VII and Ne IX agrees with the predictions of Gabriel's (1972) theory, which attributes their formation to dielectronic recombination.

1. Introduction

The observation of emission lines of highly ionized atoms provides a powerful means for studying the plasma of the solar corona. Many experiments for this purpose have been carried out with uncollimated plane Bragg spectrometers. Recent work includes that of Evans and Pounds (1968), Batstone *et al.* (1970), and Rugge and Walker (1970, 1971). All of these experiments respond to the Sun by convoluting the spatial and spectral distribution of the radiation. Parkinson (1971) has reported results of the first solar experiment with a collimated Bragg spectrometer.

In this paper we report some results of a coronal survey carried out with an X-ray spectrometer system which permitted the study of individual active regions and the general corona. In this experiment a pair of large area, collimated crystal spectrometers were used to study the resonance, intersystem and forbidden line emission from the helium-like ions O VII and Ne IX. An Oda-type collimator provided a one-dimensional

† We are saddened to report the death of A. J. Meyerott on 13 November, 1971.

Solar Physics **26** (1972) 183–201.

'fan beam' field of view of 1.7′ full width at half maximum (FWHM) in the plane of dispersion by several degrees FWHM in a direction perpendicular to the dispersion plane. While the two crystals scanned over the three lines from each of these ions, the field of view passed slowly across the solar disc twice at different heliocentric angles. The experiment was flown on a NASA-Aerobee 170 rocket from White Sands Range and collected data from approximately 1632 UT to 1637 UT on 29 April 1971.

2. Instrumentation

The instrumentation is unique in increasing sensitivity, spatial and spectral resolution at the expense of spectral range (Acton *et al.*, 1971a). Figure 1 shows a schematic representation of the payload. The two plane KAP crystals (97 cm^2 each) were mounted below the large X-ray collimators and were rotated independently in 64 steps through the small range of Bragg angles necessary to cover the wavelength ranges 21.38–22.27 Å (O VII) and 13.34–13.78 Å (Ne IX). The crystal rocking period was one second for the 64 steps. Photons diffracted from the two crystals were registered in proportional counters (crystal detectors) which remain fixed because of the small crystal motion. Pulses from these proportional counters were passed through window discriminators to reduce the background rate before being accumulated and telemetered 64 times per second in synchronism with the stepper motors which rotate the crystals. The crystal detectors were continously calibrated in flight with weak Fe^{55}

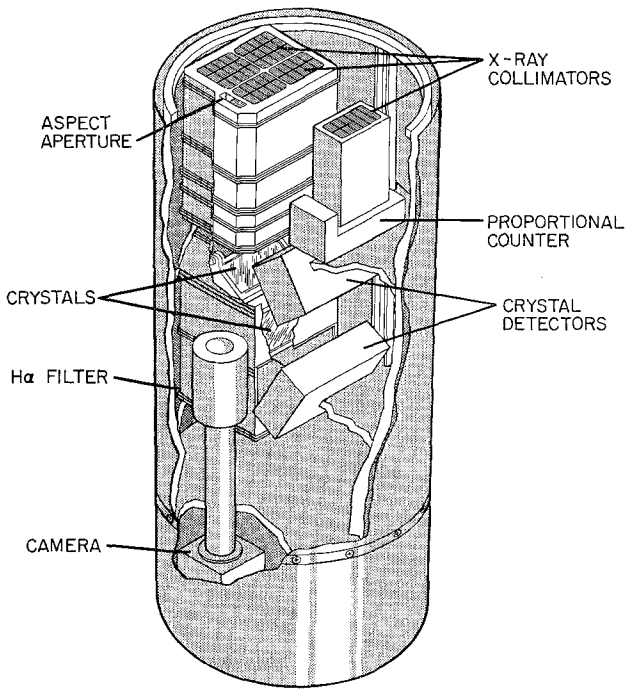

Fig. 1. A schematic view of the primary instrumentation in the rocket payload. The crystal detectors are thin window proportional counters.

sources. These calibration X-rays did not contribute to the spectrometer counting rates because of amplitude discrimination. In addition, the resonance line photon energies of 0.575 keV for O VII and 0.923 keV for Ne IX provided excellent calibration during flight.

The rocket pointing control (SPAR CS system) advanced the field of view across the solar disc at a nominal rate of 0.3′. During each complete spectral scan by the two crystals, the rocket axis moved 0.3′ or 18% of the collimator field of view of 1.7′ FWHM. Light entering an aspect aperture was directed through an Hα filter-telescope combination with a nominal 1 Å bandpass and produced a solar image on SO-392 film. An area of additional exposure approximately 4′ wide was superimposed on the solar image by light passing through the X-ray collimator grids. The location of this feature on the solar image was identical to that of the X-ray field of view on the Sun. The camera was operated at a rate of four frames per second so the motion of the collimator field of view across the solar disc could be followed throughout the flight.

A beryllium window proportional counter, sensitive in the wavelength range 0.8–4.0 Å was included in the payload. The field of view of this detector in the direction of the spatial scan was 4.2′ FWHM and was parallel to the 1.7′ field of view of the crystal spectrometers. Pulses from this proportional counter were analyzed in six differential pulse height channels. Counts were accumulated in these channels and telemetered in digital form once each second.

The payload also carried an ultravioled spectrograph utilizing a diffraction filter entrance slit. This spectrograph was provided by the Arbeitsgruppe für Physikalische Weltraumforschung, Freiburg, Germany. Preliminary results of their high resolution spectra in the 180 Å region have been reported by Schweizer and Schmidtke (1971).

3. Coronal Source Distribution

An Hα photograph of the disc, taken near the time of flight by the Lockheed Solar Observatory, is shown in Figure 2. The common field of view of the crystal spectrometers (FWHM) is represented by a pair of dashed lines. It was moved across the disc on two separate scans by the SPARCS attitude control system. The scan directions are indicated by the solid lines superimposed on the photograph. A number of plage regions are visible in Figure 2. The only transient activity on the disc at the time of flight came from a small flare ($-F$) which occured about 30 min before launch in McMath plage No. 289 near the East limb. This small dynamic feature will be discussed in detail in a later publication. No impulsive X-ray or radio events have been reported during the flight.

The wavelength resolution of the spectrometers is indicated in Figure 3 which shows spectra of both O VII and Ne IX. The spectra in this Figure were obtained during a 5 s time interval from the X-ray active region associated with plage No. 281. The resonance ($1s^2\ ^1S_0$–$1s2p\ ^1P_1$), intersystem ($1s^2\ ^1S_0$–$1s2p\ ^3P$) and forbidden ($1s^2\ ^1S_0$–$1s2s\ ^3S_1$) transitions are labelled. In 5 s the rocket axis moves 1.5′ across the disc, a

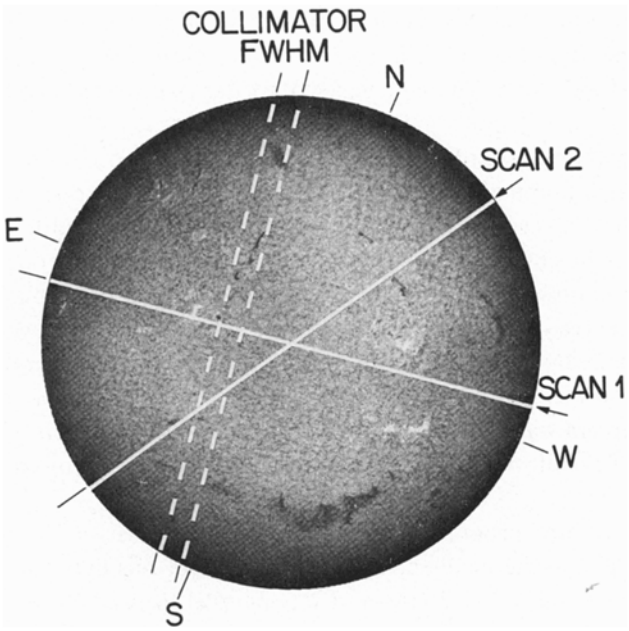

Fig. 2. A solar disc photograph in Hα taken near the time of flight by the Lockheed Solar Observatory. The scan directions and the field of view of the crystal spectrometers are indicated on the photograph.

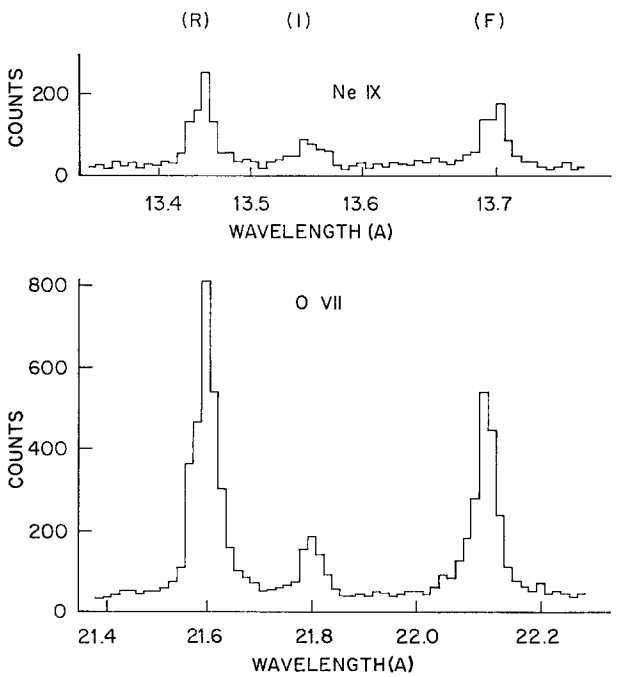

Fig. 3. O VII and Ne IX spectra of McMath plage No. 281 accumulated during flight in approximately five seconds. Resonance, intersystem and forbidden transitions are labelled R, I and F respectively.

distance approximately equal to the full width at half maximum of the collimator field of view. The data of Figure 3, therefore, demonstrate the typical sensitivity and wavelength resolution of the experiment with counts registered from one instrument field of view.

Plots of counting rate against position on the disc are shown in Figures 4 and 5 for both crystals and the proportional counter. In Figure 4, the emission from the three lines (R, I and F) has been added together for the O VII (Figure 4a) and Ne IX (Figure 4b) ions and plotted against disc position for the first rocket scan. The counting rate from four of the proportional counter energy channels (3.2–7 keV) is similarly plotted in Figure 4c. Data obtained during the second scan are plotted in Figure 5a and b. The O VII detector failed shortly after the start of the second scan and so data from these lines on the second scan are not available.

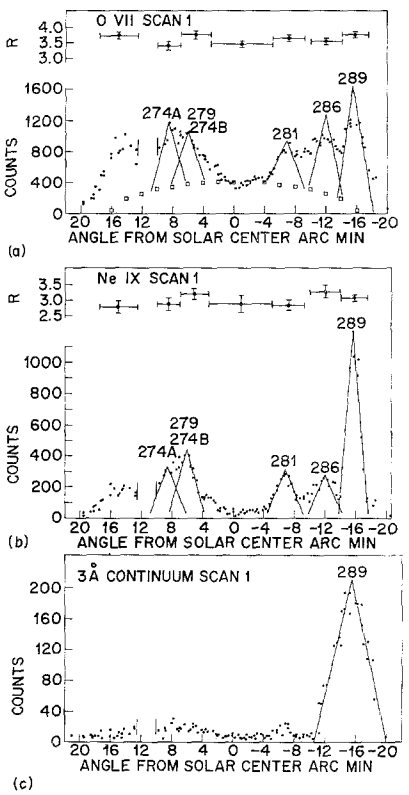

Fig. 4. Plots of the total line emission and the forbidden to intersystem line ratio (R) from O VII (a) and Ne IX (b) acquired during the first scan across the disc. The continuum near 3 Å (3–7 keV) obtained by the Be-window counter during this scan is shown in (c). The solid lines indicate the triangular shaped collimator response which has been fitted to the active region emissions with the McMath-Hulbert plage numbers of each region resolved shown above the triangles. Contribution of the general corona, extrapolated over the disc as described in the text, is shown by the small squares in part (a). The data gap at plus 10′ was caused by a momentary malfunction of the attitude control system.

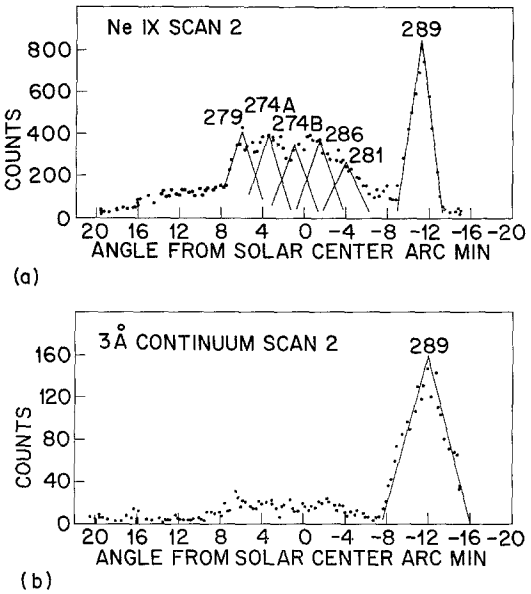

Fig. 5. Plots of total line emission against disc position for Ne IX (a) and 3–7 keV continuum (b) taken from the second rocket scan. Contribution from each active region is indicated by the McMath-Hulbert numbers above each triangle.

When the spectrometer's field of view was near the center of the disc during the first scan the collimators were pointed at a region free from plage activity. For both the O VII and Ne IX data, the counting rates dropped to a minimum at this time as shown in Figure 4a and b. The points marked by squares (□) in Figure 4a show how this signal from the 'general corona' would be modified as the fan beam field of view is moved away from the center of the disc to include less of the corona assuming the general coronal emission is uniform for the entire disc.

It may be seen from Figure 4 that X-ray active regions are more easily resolved in Ne IX radiation than in the radiation of O VII. This is because the general coronal temperature is close to the temperature of maximum abundance for O VII. In active regions, the relative emissivity of Ne IX is increased. For this reason, and because data were available from two scans, the location of the active regions was carried out using the Ne IX counting rates. The signal from the general corona was determined as described above and subtracted from the total counting rate at each point on the disc to determine the contribution of the active regions. The emission observed near the beginning of both scans comes from near the Northwest limb and was presumed to be from several diffuse plages in that area. These data were treated as a unit for calculational purposes and no further attempt was made to spatially resolve them. The other active region data were fitted to the triangular response of the collimator with the assumption that the regions were small compared to the 1.7′ collimator field of view. This process was carried out with Ne IX data from both scans and source locations on

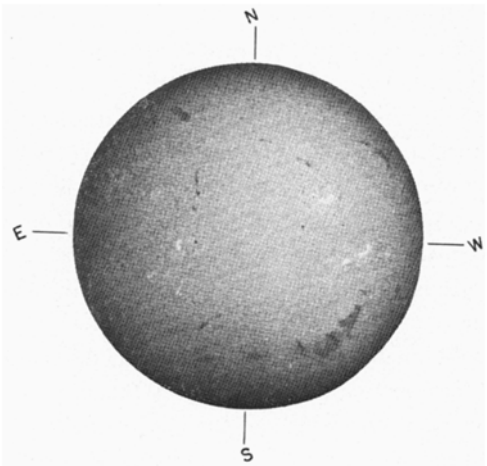

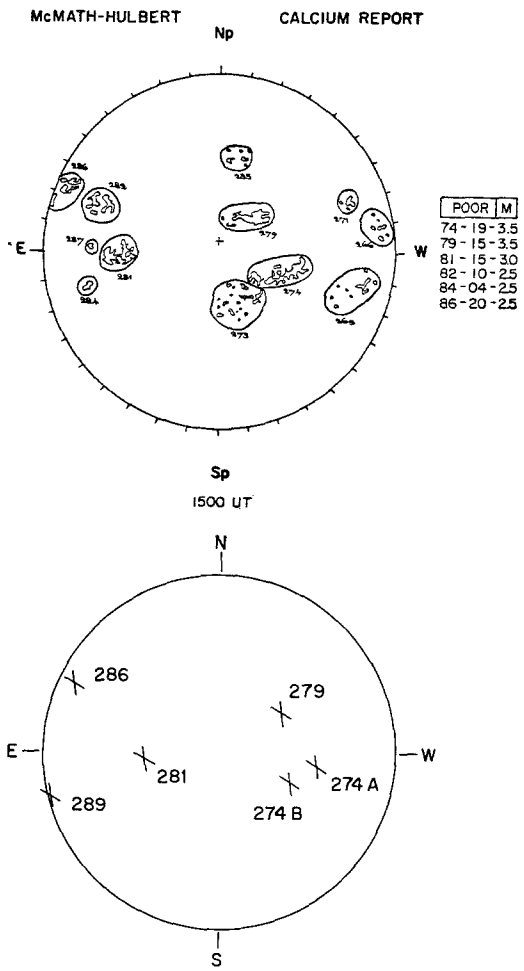

Fig. 6. The location of X-ray emitting regions on the disc are shown together with an H-alpha photograph. The McMath-Hulbert plage map is for the day before the flight.

each scan were transferred to an Hα photograph as a series of straight lines .The points of intersection of these lines were correlated with Hα features. The McMath numbers of the correlated plages are shown in Figures 4b and 5a. The source locations were then transferred to the O VII plot and the amplitude of the contribution from each active region was determined. For at least two of the regions, (286 and 289) the triangular response of the collimator does not provide a good fit to the data. Perhaps the assumption that the source size is small compared to the collimator field of view is no longer valid for O VII because the emitting regions may be more diffuse at the lower temperatures where this ion is most abundant. This point will be discussed further in connection with the values calculated for emission measure.

The source locations, obtained from the Ne IX data as described above are shown in Figure 6. A McMath-Hulbert calcium report for the previous day (April 28) is shown since no data have been published for the day of the flight. Regions 265, 266 and 271 have moved onto the West limb by April 29 and are probably responsible for the diffuse emission observed near the beginning of both scans.

Measured values of R, the ratio of the forbidden (F) to intersystem (I) line intensities are plotted in Figure 4 at various positions across the disc for both the Ne and O data. No variation is found in this ratio which may be attributed to especially high density regions (Acton *et al.*, 1971b).

Figures 4c and 5b show data from the collimated proportional counter. These data show the dominance of the small dynamic feature at higher photon energies. The emission from region 289 at these energies is at least 10 times that of any other region on the disc. The emission in the 3.2–7 keV band from this feature decreases by about 20% in the two minutes separating scans one and two.

4. Plasma Parameters

The intensity of the O VII and Ne IX resonance lines may be used to obtain information on the electron temperature and emission measure of the emitting regions. The number of counts recorded in a line during one rotation of the crystal is given by:

$$N_\lambda = F_\lambda \frac{R_\lambda}{W} t A_\lambda p_\lambda , \tag{1}$$

where N_λ is the integrated number of counts in the line per crystal scan, F_λ is the photon flux at wavelength λ in photons $cm^{-2}\,s^{-1}$, R_λ is the integrated reflection coefficient of the crystal in radians, W is the angular rotation rate of the crystal in rad s^{-1}, t is the transmission of the collimator, A_λ is the effective area of the crystal in cm^2 when it is set at the correct Bragg angle for the diffraction of X-rays of wavelength λ, and p_λ is the photon detection efficiency of the proportional counter used to register the photons diffracted from the crystal. The subscript, λ, is used to denote parameters which are wavelength dependent. The intrinsic line width is assumed small compared with the crystal rocking curve in all cases – a valid assumption for Doppler broadened lines from the coronal plasma incident on KAP crystals.

For the present analysis, we have used the KAP crystal reflection coefficients measured by Charles (1968) and by Blake (private communication, 1971). These are 1.8×10^{-5} and 5.5×10^{-5} rad for the O VII and Ne IX spectrometers, respectively. The crystal rotation rate W is 0.053 and 0.018 rad s^{-1} for the O VII and Ne IX systems respectively and the numerical value of the parameter t is 0.3. The parameters A and p have the values 52 and 0.095 for the O VII and 51 and 0.42 for the Ne IX system.

Table I presents the observational data obtained by this experiment. The counts given represent the total observed in one crystal rotation when the source is centered in the collimator field of view. The general coronal signal has been subtracted as described above and the stated errors primarily represent the uncertainty in this process. In the case of the general corona the errors reflect only counting statistics.

TABLE I

Experimental data

Plage region	Counts[a] O VII	Counts[a] Ne IX	O/Ne[b] ratio	R[c] O VII	R[c] Ne IX
289	672 ± 146	605 ± 43	1.11 ± 0.25	3.7 ± 0.1	3.1 ± 0.1
279, 274B	400 ± 73	214 ± 33	1.87 ± 0.45	3.7 ± 0.1	3.2 ± 0.2
281	365 ± 44	148 ± 17	2.47 ± 0.41	3.6 ± 0.1	2.8 ± 0.2
274A	473 ± 128	148 ± 43	3.20 ± 1.27	3.4 ± 0.15	2.9 ± 0.2
286	492 ± 73	142 ± 30	3.46 ± 0.89	3.5 ± 0.1	3.3 ± 0.2
265, 266	427 ± 47	92 ± 10	4.65 ± 0.72	3.7 ± 0.2	3.0 ± 0.3
Gen. corona	225 ± 5	21 ± 1	10.71 ± 0.56	3.4 ± 0.1	2.9 ± 0.2

[a] Counts in the resonance line ($1s^2\,{}^1S_0$–$1s2p\,{}^1P_1$) normalized to one crystal rotation and best collimator aspect.

[b] Ratio of counts recorded in the two resonance lines.

[c] Ratio of forbidden ($1s^2\,{}^1S_0$–$1s2s\,{}^3S_1$) to intersystem ($1s^2\,{}^1S_0$–$1s2p\,{}^3P$) line intensities.

In order to determine the temperature dependence of the ratio of O VII to Ne IX resonance line fluxes, it is necessary to calculate the emissivity of a coronal plasma. On the assumption that every collisional excitation of a resonance transition is followed with spontaneous decay by photon emission the line flux may be calculated with the aid of an approximate expression for the electron collisional excitation rate. The $\bar{g}$ approximation (Van Regemorter, 1962; Seaton, 1964) for the line flux is given by:

$$F_\lambda = 5 \times 10^{-31}\, \bar{g} f_\lambda \varphi_\lambda^{-1} A_z \int M A_i T^{-0.5}\, 10^{-(5040\varphi_\lambda/T)}\, \mathrm{d}T \qquad (2)$$

photons $cm^{-2}\, s^{-1}$ at Earth.

In this expression $\bar{g}$ is the temperature averaged Gaunt factor (which has been set equal to 0.3), f_λ is the oscillator strength of the line, φ_λ is the photon energy in electron volts, A_z is the elemental abundance relative to hydrogen, M is the differential emission measure, T is the electron temperature in degrees Kelvin but to be consistent with our definition of M the integration step $\mathrm{d}T$ has the dimension 10^6 K. A_i is the ion abundance at temperature T. Values of A_z for neon (2.8×10^{-5}) and oxygen (5.9×10^{-4}) were obtained from Dupree (private communication, 1971). The ionization balance calculations of Jordan (1969) provided the temperature dependent ion abundances.

The numerical constant includes a factor relating the electron and hydrogen densities. The constant given is for a helium abundance of about 0.1. The emission measure of a volume is normally defined as $\int N_e^2 \, dV$, the integral of the square of the local electron density over the volume of interest. The local electron density, N_e, may alternatively be expressed as a function of the local electron temperature within the volume of interest. Thus, the differential emission measure, $M(T)$, is defined:

$$M(T) = \frac{d}{dT} \int N_e^2 \, dV \text{ cm}^{-3} (10^6 \text{ K})^{-1}. \tag{3}$$

With two resonance line intensities and Equations (1) and (2) one may derive two parameters descriptive of the coronal plasma. For instance, if an isothermal model is assumed, the ratio of line intensities may be used to derive the electron temperature. The temperature is put back into the equations along with the absolute flux of either line to give the corresponding emission measure. Alternatively, one may assume some functional form for the differential emission measure and use the observations to solve for the functional parameters.

We have analyzed the data by both methods. For the emission measure distribution in the non-isothermal case, the exponential expression

$$M(T) = C \times 10^{-T/T_0} \text{ cm}^{-3} (10^6 \text{ K})^{-1} \tag{4}$$

proposed by Chambe (1971) has been adopted. Here T is the electron temperature and the constants C and T_0, which are related to the total emission measure and the steepness of the emission measure distribution, are parameters determined from the analysis. Such a distribution appears to be consistent with the data of Batstone *et al.* (1970). However, the value for T_0 which we derive from their data on three active regions is approximately 7×10^6 K, a value somewhat higher than Chambe's $1.5\text{–}3 \times 10^6$ K.

In Figure 7 the calculated O VII/Ne IX resonance line ratio for our spectrometers is plotted versus T (for the isothermal case) and T_0 (for the exponential distribution). Note that in the case of the exponential distribution of emission measure the minimum ratio is more than ten times larger than in the isothermal case. This is a consequence of the large amount of low temperature material always present to produce the O VII line in this model.

The results of the isothermal approximation are given in Table II. The derived electron temperatures have a formal uncertainty of about 10^5 K arising from the experimental errors in the data of Table I. The inadequacy of the isothermal model and possible systematic errors introduce additional uncertainty in the derived plasma parameters. The electron temperatures of the quiescent active regions cluster about a common value with the general corona substantially cooler. The emission measure for the general corona contains a factor of 20 relating our field of view to the whole coronal hemisphere on the basis of a spherically symmetric model. The general coronal temperature is consistent with that derived by Jordan (1966) from EUV data but below the value of 1.8×10^6 K obtained by Withbroe (1971) from a study of Li-like line ratios. Widing and Sandlin (1968) have found that the spectrum in the 61–110 Å

region is best fitted to a general coronal temperature of 1.4×10^6 K but comment that all of their data cannot be fitted by an isothermal model. The temperature of 2.4×10^6 K and the associated emission measure for the dynamic feature of region 289 are insufficient to produce the observed emission at energies from 3.2–7 keV. Material at

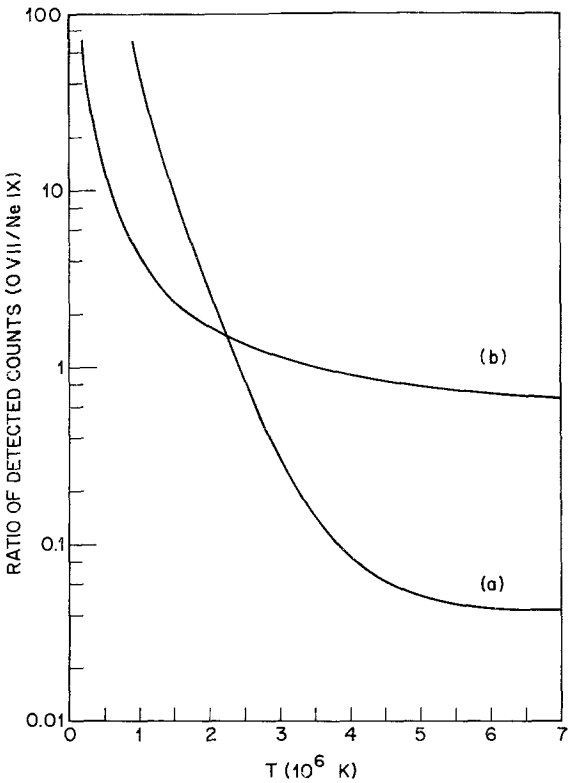

Fig. 7. The ratio of O VII to Ne IX resonance line counts plotted against electron temperature for an isothermal model (a) and against the parameter T_0 of Equation (4) for a model (b) in which the emission measure decreases exponentially with a slope determined by T_0.

TABLE II

Isothermal model

Plage region	Electron temperature (10^6K)	Emission measure (10^{47} cm^{-3})
289	2.40	16
279, 274B	2.15	8
281	2.05	7
274A	1.95	9
286	1.90	9
265, 266	1.80	8
Gen. corona	1.45	140[a]

[a] Emission measure of coronal hemisphere facing the Earth.

a considerably higher temperature is required to explain this emission which serves to emphasize the inadequacy of the isothermal model.

The temperatures given in Table II for the isothermal model are in general lower than the preliminary values given by Catura *et al.* (1972) on the basis of the same experimental data. The reason for the difference is that the earlier values were derived using the peak KAP crystal reflectivities of Liefeld *et al.* (1970). Liefeld's results are based on measurements using a double crystal spectrometer. A correction for polarization effects and convolution of the two rocking curves must be applied if these data are to be used in analysis of single crystal measurements. When such corrections are applied there remains a disagreement of a factor of approximately two between the reflection coefficients of Liefeld *et al.* (1070) and those of Charles (1968) and Blake (private communication, 1971). Because of this confusion, and because of the difficulty in relating two crystal measurements to collimated single crystal measurements, we have chosen to reinterpret our data on the basis of integrated reflection coefficients as given by Equation (1). This approach also facilitates comparison with earlier work.

The exponential distribution of emission measure in Equation (4) (Chambe, 1971) provides a means for treating the emission of non-isothermal regions. The data of Table I and the appropriate curve of Figure 7 have been used to derive the parameters given in Table III for each region. Although T_0 has the dimensions of a temperature, it is merely a scaling factor and its absolute value depends on the choice of 10 as the base of the exponential function. Once T_0 has been determined, the observed intensity in the resonance line and the solution of Equations (1), (2) and (4) may be used to determine the constant C of Equation (4).

The mean emission temperature, $\langle T_\lambda \rangle$, for each ion is defined

$$\langle T_\lambda \rangle = \frac{\int T B_\lambda \, dT}{\int B_\lambda \, dT} \text{ K}, \tag{5}$$

TABLE III

Non-isothermal (exponential) model

Plage region	T_0 (10^6 K)	C[a]	EM_{tot}[b] (10^{47} cm^{-3})	$\langle T_{O\,VII} \rangle$ (10^6 K)	$\langle T_{Ne\,IX} \rangle$ (10^6 K)	$EM_{Ne\,IX}$ (10^{47} cm^{-3})
289	3.15	3	23	1.95	3.10	13
279, 274B	1.80	6	13	1.80	2.70	5
281	1.50	8	12	1.70	2.55	4
274A	1.25	18	16	1.65	2.40	4
286	1.15	24	16	1.60	2.30	4
265, 266	0.95	42	15	1.50	2.20	3
Gen. corona[c]	0.60	170	170	1.25	1.70	10

[a] The constant of Equation (4). Units: 10^{48} cm^{-3}(10^6 K)$^{-1}$.

[b] Emission measure above 10^6 K. Essentially equal to O VII emission measure.

[c] All values refer to coronal hemisphere facing the Earth.

where B_λ is the integrand of Equation (2) with M in the form of Equation (4). The emission measure for each ion, EM_λ, is given by:

$$EM_\lambda = \int_{T_1}^{T_2} M \, dT \text{ cm}^{-3}, \tag{6}$$

where the limits of integration have been arbitrarily set at the temperatures where the emissivity of the gas for the particular resonance line is 10% of its peak value. The emission measure defined in this way has a wavelength dependence which enters through these limits of integration. The total emission measure of each region, EM_{tot}, is obtained by integrating Equation (6) from 10^6 K to ∞. The lower temperature limit is arbitrarily set to approximate the temperature at the base of the corona.

The errors in T_0 are in general unsymmetrical because of the shape of the curve in Figure 7. These errors are on the average 30% on the high temperature side and 15% on the low temperature side. The mean emission temperatures given in Table III are in general determined to better than 10% and the emission measures to about plus or minus 50%.

Because the exponential function of Equation (4), the basis of our non-isothermal model, decreases monotonically toward higher temperatures, the derived emission measures of Table III are naturally greater for O VII, the ion formed at the lower temperature. However, this result is consistent with the data of Figure 4 which show that the O VII regions are larger than the Ne IX regions, relative to our 1.7′ FWHM field of view. For example, taking a typical O VII emission measure of 1.6×10^{48} cm^{-3} and a mean emission temperature of 1.6×10^6 K from Table III and an electron density of 2×10^9 cm^3 from the results of Section 5, and assuming a uniform source region one scale height (3.5×10^4 km) thick, we find that the characteristic lateral dimension of the O VII regions are of the order of 2′. For a similar geometrical model and electron density the characteristic lateral extent of the Ne IX regions turns out to be about 1′. Such source sizes are consistent with the data of Figure 4. These results are not unique to the particular non-isothermal model chosen but it is clear that a model is required for which the source regions are more compact at shorter wavelenghts.

5. Spectra

The high sensitivity of our instrument has provided spectra of high statistical accuracy. Also, the narrow collimation employed limited degradation of the spectra resulting from source extent. For this study, the spectra of Figure 8 have been obtained by summing together all useable data from the flight, excluding only that from the dynamic feature associated with plage 289.

Analysis of these spectra is complicated by the possible presence of unknown line blends in the data and by lack of presicion in the published wavelengths of the known lines. Furthermore, we do not have a detailed rocking curve for the flight crystals and attempts to derive such a curve from the flight spectra have been only partially success-

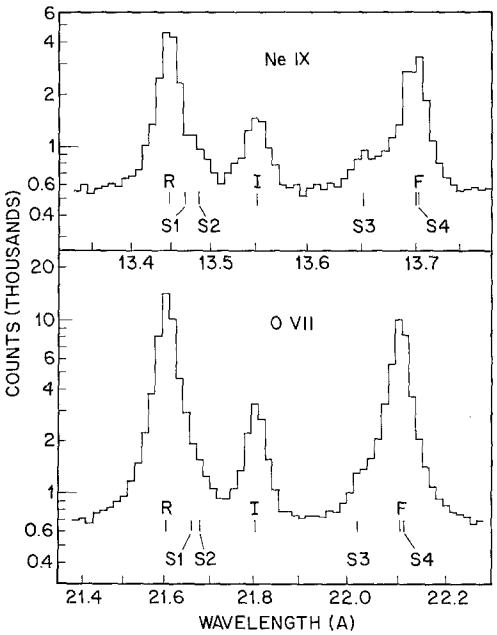

Fig. 8. Spectra summed to include all useful data from both scans of the disc but excluding the flaring region (plage 289). Position of reported satellite lines are indicated by S1–S4. Line widths of the Ne IX lines are determined by the collimation while those of O VII are essentially the rocking curve of the KAP crystal. Intersystem line of Ne IX is broadened relative to R or F lines by the fine structure of this transition or because of an unreported blend. The double width steps seen at 13.47 and 13.69 in the Ne IX spectra are caused by the treatment of these data in the flight data processor and not by errors in the crystal scan.

ful. The rocking curve is found to be unsymmetrical; near the peaks the line profiles drop off more steeply on the long wavelength side in agreement with theory (Compton and Allison, 1935).

Results of our analysis are presented in Table IV. Except where noted the wavelengths are determined from the laboratory angular calibration of the spectrometer scans. These were normalized at the given wavelegth of the resonance lines. Except for possible unknown systematic errors, these relative wavelengths are estimated to be accurate to 0.004 Å for the O VII system and 0.002 Å for Ne IX. The wavelengths derived for the I and S3 lines of Ne IX are in better agreement with the interpolated values from Flemberg's (1942) data than previous values which are summarized by Parkinson (1971) and Walker and Rugge (1970). The derived wavelengths are in excellent agreement with the recent theoretical work of Gabriel (1972) when the Ne IX wavelength scale is re-normalized to his resonance line wavelength.

According to the theory of Gabriel (1972) the upper level of the S3 satellite line is formed by dielectronic recombination and the strength of this line relative to the resonance line decreases approximately as the inverse square of the electron temperature for the range of temperatures encountered in Table III. We have scaled S3/R

TABLE IV

Spectra

Line (Figure 9)	Transition	λ–O VII (Å)	Relative strength[b] This work		λ–Ne IX (Å)	Relative strength[b] This work	
R	$1s^2\,{}^1S_0$–$1s2p\,{}^1P_1$	21.602			13.447		
S1		21.642[a]	$\lesssim 0.04$		13.469[a]	~ 0.06	0.016[a]
S2		21.677[a]			13.488[a]		0.012[a]
I	$1s^2\,{}^1S_0$–$1s2p\,{}^3P_{1,2}$	21.805			13.551		
S3	$1s^22s^2S^e$–$1s2p2s^2P^0$	22.024	~ 0.025	< 0.04[a]	13.651	~ 0.09	~ 0.04[a]
F	$1s^2\,{}^1S_0$–$1s2s\,{}^3S_1$	22.103			13.700		
S4	$1s^22p^2P^0$–$1s2p2p^2D^e$	22.108[a]			13.703[a]		

[a] Parkinson (1971).
[b] Strength of satellite line(s) relative to resonance line.

ratios from Gabriel's theoretical curves for O VII and Ne IX at temperatures corresponding to the mean emission temperatures of Table III. Weighted averages of these S3/R ratios were computed with weights assigned according to the relative counts recorded from each region as given in Table I (listed general corona counts were multiplied by 20 to include entire hemisphere). These average S3/R ratios may be compared directly with the experimental values of Table IV which are derived from the integrated spectra of Figure 8. The computed ratios are 0.025 and 0.08 for O VII and Ne IX respectively. Such precise agreement with the observed ratios is fortuitous but lends credance to Gabriel's theory.

The S3/R ratios averaged as above but for the isothermal temperatures from Table II are 0.018 for O VII and 0.115 for Ne IX. Thus agreement with the observations is poorer in the case of the isothermal model and for Ne IX this disagreement is larger than our estimated experimental error.

The work of Gabriel and Jordan (1969) demonstrated that the ratio, R, of the intensities of the forbidden (F) to the intersystem (I) lines of helium-like ions is sensitive to electron density for sufficiently high densities. More recently, Freeman *et al.* (1971) and Blumenthal *et al.* (1971) have reconsidered the problem.

The values of R derived from our data for different coronal features are given in Table I and indicated in Figure 4. We have concluded earlier (Acton *et al.*, 1971b) on the basis of these data that the absence of statistically significant variations among the R values implies that all regions observed are below the low density limit of 6×10^9 cm^{-3} given by Freeman *et al.* (1971). It is worth re-examining these data in view of the work of Blumenthal *et al.* (1971) which explicitly includes temperature dependent effects.

For the case in which the radiative excitation of the $1s2p\ {}^3P$ levels from $1s2s\ {}^3S_1$ is negligible, the dependence of the electron density, N_e, on R may be conveniently written

$$N_e = N_c\left[(R_0/R) - 1\right] \mathrm{cm}^{-3}. \tag{7}$$

Blumenthal *et al.* (1971) give curves of R_0 and N_e versus temperature for O VII. Their pedicted variation of R_0, the low density limit of R, for the $1\text{–}2 \times 10^6$ K range is reproduced as a solid line in Figure 9. Over this range their value of N_e is approximately constant at 3.4×10^{10} cm^3. Also plotted in Figure 9 are the R values from Table I versus the mean temperature of O VII line formation from Table III. Although the experimental accuracy is limited the experimental R values tend to follow the trend of the R_0 curve but to fall systematically below it. For the apparent decrease of R below R_0 of about 5% Equation (7) indicates that the electron density within the O VII line forming portions of the active regions is of the order of 2×10^9 cm^{-3}.

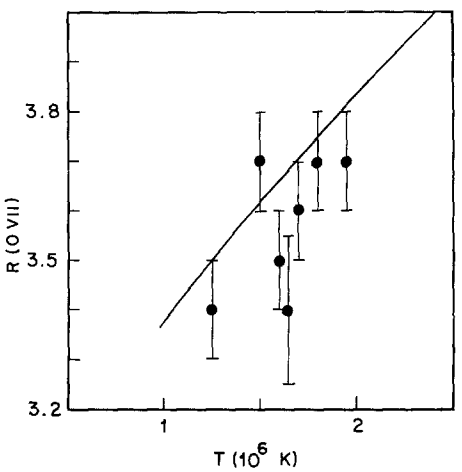

Fig. 9. The solid curve is the forbidden to intersystem line ratio in the low density limit (R_0) taken from Blumenthal *et al.* (1971). It is plotted versus the electron temperature of the line forming region. The experimental data points are the O VII R values for the coronal regions listed in Table I. In this case, the abcissa is $\langle T_{O\ VII} \rangle$, the corresponding mean emission temperatures from Table III.

The values of the parameter G, the ratio of forbidden plus intersystem lines to the resonance line, for the data of Figure 8 are 0.92 ± 0.01 and 0.90 ± 0.02 for O VII and Ne IX respectively. Corrections have been applied for the S4 satellite line under the assumption that it is equal in strength to S3 (Gabriel, 1972). The quoted errors are purely statistical.

6. Summary and Conclusions

The results of this rocket experiment show that much of the X-ray line emission from the solar corona may be unambiguously associated with corona overlying calcium plages. After the radiation from these compact regions has been accounted for, there remains a residual signal which is attributed to diffuse emission from above old plages and from the general corona. The compactness and contrast of the coronal sources increase with increasing energy. In this regard the coronal structures inferred from

our monochromatic measurements are consistent with those seen on heterochromatic X-ray photographs obtained with high-resolution imaging systems. (Van Speybroeck *et al.* 1970).

The changing geometry of the source regions with photon energy as well as the X-ray spectrometery of Batstone (*et al.* 1970) indicate a need to go beyond a simple isothermal model in the interpretation of line ratio data. On the basis of an assumed emission measure distribution which varies as an inverse exponential with electron temperature, the following characteristics of the coronal plasma have been derived.

(1) The decrease of the emission measure with temperature is 2–3 times as steep in the general corona as it is over active regions. Furthermore, the decrease of emission measure with temperature in a small dynamic feature is only one-half as steep as in the quiescent active regions.

(2) Although there is a spread in T_0 among the active regions, they seem to cluster around a value giving a tenfold decrease in emission measure for a 1.4×10^6 K increase in temperature. This fact, when considered with the small signal observed from these regions by the proportional counter spectrometer, is not compatible with the results of Batstone *et al.* (1970). We conclude that the three active regions which they describe are all higher energy features.

(3) Under the assumption of spherical symmetry, we find the rms electron density in the general corona is of the order of 4×10^8 cm^{-3}. The total emission measure of the coronal hemisphere above 10^6 K is about 2×10^{49} cm^{-3}. This value is in agreement with that derived by Elwert (1954) on the basis of the Baumbach model of the quiet corona.

(4) The active regions contribute about one-third of the total coronal emission measure but less than 5% of the total coronal material.

We find that the trend with temperature of the ratio, R, of the forbidden to intersystem lines for O VII agrees with the work of Blumenthal *et al.* (1971). Although it is at the limit of our experimental accuracy, the apparent systematic departure of R below Blumenthal's R_0 may be interpreted as indicating densities of the order of 2×10^9 cm^{-3} in the O VII emitting portions of active regions. This electron density with the total emission measures of Table III indicates emitting volumes of the order of 4×10^{29} cm^3 for characteristic dimensions of 2′. This is consistent with the data of Figure 4a which show the O VII sources to be somewhat extended compared to the 1.7′ field of view.

Comparison of the S3 satellite to resonance line ratios from our integrated O VII and Ne IX spectra with suitably averaged theoretical values from Gabriel's (1972) work relating satellite strength to dielectronic recombination shows good agreement for data reduced on the basis of the non-isothermal model which we have used. Discordant results are obtained when the comparison is based on data reduced according to an isothermal approximation.

Wavelengths have been assigned to the principal emission lines in the 13.34–13.78 and 21.38–22.27 Å ranges based on the angular scan calibration of our Bragg spectrometers. In general, these wavelengths agree well with previous results (Walker and Rugge, 1970; Parkinson, 1971). Wavelengths for the intersystem and one of the satel-

lite lines of Ne IX are in better agreement with interpolated predictions than previous results.

Acknowledgements

This work has been supported by the National Aeronautics and Space Administration under contracts NASw 1834 and NAS2-6723 and by the Lockheed Independent Research Program. We are indebted to the following institutions for their ground-based support of our experiment: Aerospace Corporation, Big Bear Solar Observatory, Lockheed Solar Observatory, Mauna Loa Observatory, Mees Solar Laboratory, Sacramento Peak Observatory and the Space Environment Services Center in Boulder. We wish to thank Dr Alan H. Gabriel of Culham Laboratory for the use of his materials in advance of publication.

R. Caravalho, C. W. Gilbreth, A. S. Knapp, D. T. Roethig, and K. L. Smith of Lockheed made important technical contributions to this project. We acknowledge the excellent technical support provided by Ames Research Laboratory, Vehicle Guidance and Control Branch (SPARCS, vehicle instrumentation), and Goddard Space Flight Center Sounding Rocket Division (vehicle support) and the launch and rage and recovery support coordinated by Mr Lloyd Briggs at White Sands Missile Range.

L. W. Acton enjoyed the hospitality of the Arbeitsgruppe für Physikalische Weltraumforschung in Freiburg, Germany, during the preparation of this paper.

Note added in proof: It has been pointed out to us by Dr Carole Jordan that the mean emission temperature $\langle T_\lambda \rangle$ for O VII given in Table III for the general corona (i.e., 1.25×10^6 K) may be unrealistically low because its determination is unduly influenced by the low temperature end of the exponential emission measure distribution (Equation (4)). Physically, this is a valid criticism. However, it is not possible to devise any distribution of emission measure, including an exponential distribution arbitrarily truncated on the low temperature end, which may be used with our data to obtain a mean emission for O VII higher than that derived from an isothermal model (i.e., 1.45×10^6 K).

References

Acton, L. W., Catura, R. C., Culhane, J. L., and Meyerott, A. J.: 1971a, in F. Labuhn and R. Lüst (eds.), 'New Techniques in Space Astronomy', *IAU Symp.* **41**, 181.

Acton, L. W., Catura, R. C., Meyerott, A. J., and Culhane, J. L.: 1971b, *Nature* **233**, 75.

Batstone, R. M., Evans, K., Parkinson, J. H., and Pounds, K. A.: 1970, *Solar Phys.* **13**, 389.

Blumenthal, G. R., Drake, G. W. F., and Tucker, W. H.: 1971, *Astrophys. J.* **172**, 205.

Catura, R. C., Acton, L. W., Culhane, J. L. and Meyerott, A. J.: 1972, presented at the Third Symposium on Ultraviolet and X-Ray Spectroscopy of Astrophysical and Laboratory Plasmas, Utrecht, August 1971 (Summary to be published in *Space Sci. Rev.*).

Chambe, G.: 1971, *Astron. Astrophys.* **12**, 210.

Charles, M. W.: 1968, Thesis, University of Leicester, Leicester, England.

Compton, A. H. and Allison, S. K.: 1935, *X-Rays in Theory and Experiment*, D. Van Nostrand Co., Princeton.

Elwert, G.: 1954, *Z. Naturforsch.* **9a**, 637.

Evans, K. and Pounds, K. A.: 1968, *Astrophys. J.* **152**, 319.

Flemberg, H.: 1942, *Ark. Mat. Astron. Fys.* **28A**, 1.

Freeman, F. F., Gabriel, A. H., Jones, B. B., and Jordan, C.: 1971, *Phil. Trans. Roy. Soc. Series A* **270**, 127.
Gabriel, A. H.: 1972, submitted for publication to *Monthly Notices Roy. Astron. Soc.*
Gabriel, A. H. and Jordan, C.: 1969, *Monthly Notices Roy. Astron. Soc.* **151**, 141.
Jordan, C.: 1966, *Monthly Notices Roy. Astron. Soc.* **132**, 463.
Jordan, C.: 1969, *Monthly Notices Roy. Astron. Soc.* **142**, 501.
Liefeld, R. J., Hanzely, S., Kirby, T. B., and Mott, D.: 1970, *Adv. X-Ray Anal.* **13**, 378.
Parkinson, J. H.: 1971, Thesis, University of Leicester, Leicester, England.
Rugge, H. R. and Walker, A. B. C.: 1970, *Solar Phys.* **15**, 372.
Rugge, H. R. and Walker, A. B. C.: 1971, *Solar Phys.* **18**, 244.
Schweizer, W. and Schmidtke, G.: 1971, *Astrophys. J. Letters* **169**, L27.
Seaton, M. J.: 1964, *Planetary Space Sci.* **12**, 55.
Van Regemorter, H.: 1962, *Astrophys. J.* **136**, 906.
Van Speybroeck, L. P., Frieger, A. S., and Vaiana, G. S.: 1970, *Nature* **227**, 818.
Walker, A. B. C. and Rugge, H. R.: 1970, *Astron. Astrophys.* **5**, 4.
Widing, K. G. and Sandlin, G. D.: 1968, *Astrophys. J.* **152**, 545.
Withbroe, G.: 1971, *Solar Phys.* **18**, 458.